# Accepted Manuscript

Adsorption and photocatalytic degradation of Methylene Blue over Hydrogen-Titanate nanofibres produced by a peroxide method

Ibrahim El Saliby, Laszlo Erdei, Jong-Ho Kim, Ho Kyong Shon
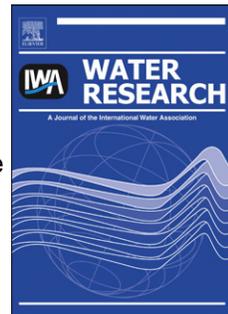
Please cite this article as: El Saliby, I., Erdei, L., Kim, J.-H., Shon, H.K., Adsorption and photocatalytic degradation of Methylene Blue over Hydrogen-Titanate nanofibres produced by a peroxide method, *Water Research* (2013), doi: 10.1016/j.watres.2012.12.045.

Adsorption and photocatalytic degradation of Methylene Blue (MB) over Hydrogen-Titanate nanofibres produced by a peroxide method

Graphic abstract
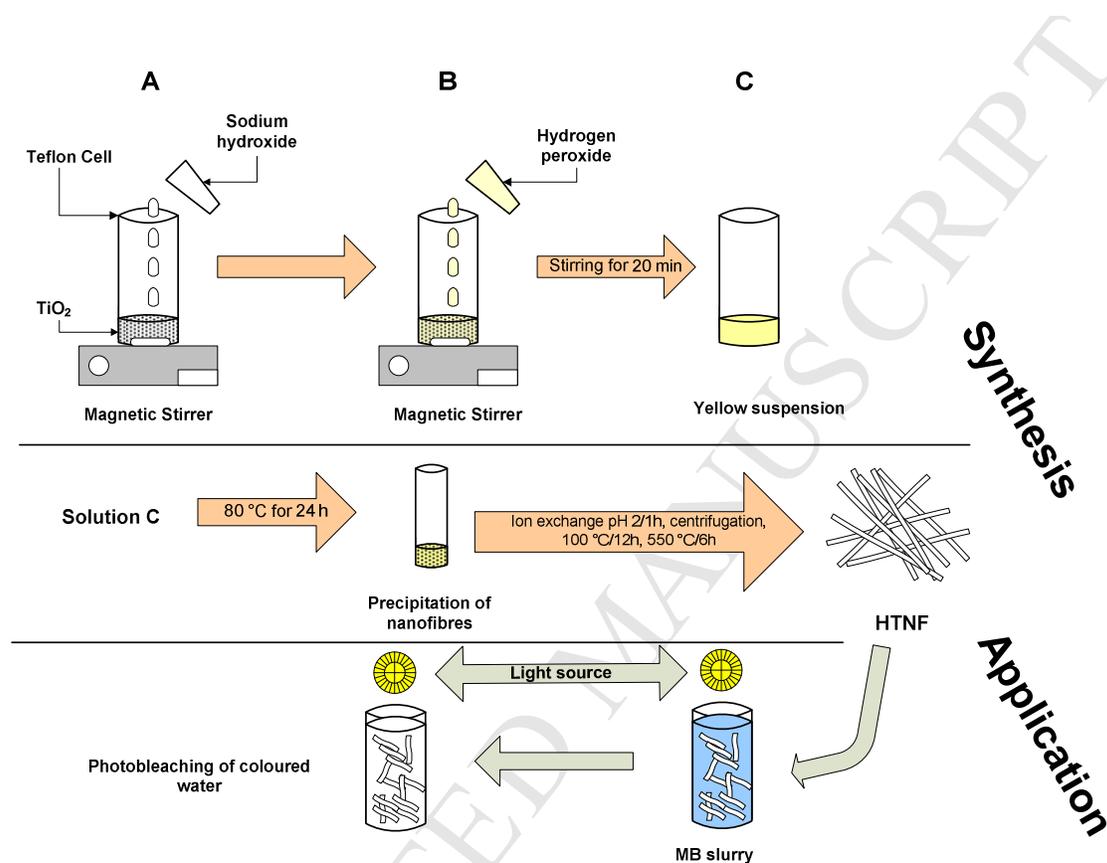
The different steps of fabrication of HTNF using the peroxide method at a low hydrothermal temperature and their use in the photobleaching of coloured water.

1 **Adsorption and photocatalytic degradation of Methylene Blue over Hydrogen-Titanate**

2 **nanofibres produced by a peroxide method**

3

4 Ibrahim El Saliby[1], Laszlo Erdei[2], Jong-Ho Kim[3] and Ho Kyong Shon[1*]

5

6 [1]Faculty of Engineering and Information Technology, University of Technology, Sydney

7 (UTS), PO Box 123, Broadway, 2007 Australia

8 [2]Faculty of Engineering and Surveying, University of Southern Queensland, QLD 4350,

9 Toowoomba, Australia

10 [3]School of Applied Chemical Engineering, Chonnam National University, Gwangju 500-757,

11 Korea

12

13 Email addresses: ibrahim.elsaliby@uts.edu.au (I. El Saliby), laszlo.erdei@usq.edu.au (L.

14 Erdei), jonghkim@chonnam.ac.kr (J.-H. Kim), hokyong.shon-1@uts.edu.au (H.K. Shon),

15

16 * Corresponding author: Tel: +61 2 9514 2629, fax: +61 2 9514 2633

17

18 **Abstract**

19

20 In this study, Degussa P25 TiO_2 was partially dissolved in a mixture of hydrogen peroxide

21 and sodium hydroxide at high pH. The fabrication of nanofibres proceeded by the

22 hydrothermal treatment of the solution at 80 °C. This was followed by acid wash in HCl at

23 pH 2 for 60 min, which resulted in the formation of hydrogen-titanate nanofibres. The

24 nanofibres were annealed at 550 °C for 6 h to produce crystalline anatase nanofibres. The

25 nanofibres were characterised for physico-chemical modifications and tested for the

26 adsorption and photocatalytic degradation of methylene blue as a model water pollutant. An

27 average specific surface area of 31.54 m^2/g, average pore volume of 0.10 cm^3/g and average

28 pore size of 50 Å were recorded. The nanofibres were effective adsorbents of the model

29 pollutant and adsorbents and good photocatalysts under simulated solar light illumination. No

30 reduction in photocatalytic activity was observed over three complete treatment cycles, and

31 the effective separation of nanofibres was achieved by gravity settling resulting in low

32 residual solution turbidity.

33

1. Introduction

The use of titania nanoassemblies in the treatment of contaminated water have provided a solution to the problem encountered during the separation of nanoparticles from water. Even though "traditional" nanoparticles showed better apparent photocatalytic activity, their separation from the suspension remains the major challenge for process up-scaling. Therefore, the use of relatively large titanate nanoassemblies has become more popular because they can be easily removed from the solution.

The production of titanate nanostructures using a peroxo-titanus solution has been discussed by several authors (Mao et al., 2006; Nyman and Hobbs, 2006), and the application of Na-titanates in the adsorption and photocatalytic removal of Methylene Blue (MB) was recently reported (El Saliby et al., 2011a). Titanate nanostructures can effectively adsorb dye molecules due to their high surface area and special characteristics (Lee et al., 2007; Baiju et al., 2009; Xiong et al., 2010). The effect of synthesis temperature (Lee et al., 2008a), and sodium content (Lee et al., 2008b) on the cation exchange capacity of titanate nanotubes were reported. It was found that the increase of sodium content in the nanotubes increases the adsorption of dye through cationic exchange. Na^+ can be replaced by H^+ in the nanostructure framework by washing the Na-titanates in an HCl solution (Wei et al., 2004; Zhu et al., 2004; Mao et al., 2006; Bela et al., 2010). Belaet al. (2010) reported that the ion exchange in the titanate nanobelts was highly dependent on the duration of acid wash. The authors found that the acid wash of titanate nanobelts in a 0.1 M HCl solution for 72 h was enough to completely exchange Na^+ for H^+.

The adsorption of MB on TiO_2 nanoparticles from aqueous solution was studied by Fetterolf et al. (2003). The authors found that the Langmuir adsorption model is adequate for representing the adsorption of MB, which was attributed to electrostatic attractions. Similarly, Xiong et al. (2010) studied the adsorption of MB on titanate nanotubes and reported that the Langmuir model was appropriate for describing the monolayer adsorption mechanism.

In a recent study, MB adsorption on titanate nanostructures has been found to significantly affect the degradation of the dye under UV light (Xiong et al., 2011). Better photocatalytic decomposition was achieved in the adsorption/photocatalysis system compared to the adsorption followed by photocatalysis system under UV irradiation.The adsorption of dye molecules onto titanate nanostructures can be of significant importance in terms of initiating the dye sensitization mechanism. This can be used in solar light treatment systems that treat dye contaminated wastewater.Thus, the objectives of this study were to:

- ➢ Synthesise H-titanates nanofibres by a peroxide method and study their morphology and physico-chemical characteristics.
- ➢ Investigate the kinetics of MB adsorption on the nanofibres and carry out photocatalytic degradation of MB under simulated solar light.
- ➢ Test the photocatalytic stability and the ease of separation of the produced nanofibres.

2. Experimental Investigations

2.1. Synthesis

H-titanate nanofibres were fabricated by the same method described elsewhere (El Saliby et al., 2011b). In a typical synthesis, 2 g of Degussa P25 powder was dispersed in 12 mL of H_2O_2 (50%) under alkaline conditions by adding 4 g of NaOH (final pH 13). Later on, the mixture was placed in a Teflon cell at 80 °C for 24 h. After hydrothermal treatment, the pH of the Na-titanates suspension was decreased to pH 2 by using 1 N HCl, at which ion exchange (Na^+ and H^+) was carried out for 60 min under magnetic stirring. This was followed by washing with Milli Q (MQ) water until a pH of 7. The as-prepared nanofibres were dried in oven at 100 °C for 12 h and annealed at 550 °C for 6 h to obtain anatase nanofibres. H-titanate anatase nanofibres will be named hereafter as HTNF.

2.2. HTNF Characterisation

Morphology and elemental composition analyses of HTNF were carried out using the Zeiss Supra 55VP SEM/EDS operating at 20 kV. X-ray diffraction (XRD) patterns were generated on MDI Jade 5.0 X-ray diffractometer. Brunauer, Emmet and Teller (BET) surface area analyses were performed on an automated surface area analyser (Micromeritics Gemini 2360, USA) by means of nitrogen adsorption-desorption. The zeta potential of as-prepared and calcined powders was determined by dispersing the nanofibres in MQ water under variable

101   pH (adjusted by 0.1 N HCl or NaOH) and measured using the Malvern nano-series (Nano-zs,

102   Malvern Instruments Limited, UK) analyser.

103

104   **2.3.   MB Adsorption Experiments**

105

106   MB powder was dissolved in MQ water to prepare a stock solution of 1 g/L concentration.

107   All experimental MB solutions were prepared from the stock solution by dilution. The dark

108   adsorption experiments were performed in 250 mL conical glass Erlenmeyer flasks

109   containing 100 mL of the desired MB solution. The flasks were enwrapped in aluminium foil

110   to prevent the illumination of slurries by ambient light. The homogeneity of suspensions was

111   maintained by placing the flasks in an orbital shaking incubator (Thermoline, TU400) at a set

112   temperature of 25 °C and a shaking speed of 150 rpm unless otherwise stated. Samples were

113   collected at designated time intervals, filtered through 0.45 μm polytetrafluoroethylene

114   (PTFE) membrane syringe filters, and analysed for colour removal by measuring absorbance

115   at the maximum absorbance wavelength of MB ($\lambda = 664$ nm) using a Shimadzu UV-Vis 1700

116   spectrophotometer. The concentration of MB (mg/L) was calculated by the following

117   equation:

118

119    $$C_t = \frac{Abs_t}{Abs_0} C_0$$ (Eq. 1)

120

121   where, C_t (mg/L) is the concentration of MB at time t, C_0 (mg/L) is the initial concentration

122   of MB, Abs_t and Abs_0 are absorbance values for $\lambda = 664$ nm at time t and 0, respectively.

123

124   2.3.1. Effect of HTNF Loading

125

126   In this experiment, five different powder loadings (0.1, 0.2, 0.5, 1 and 2 g/L) were selected to

127   study the adsorption of MB molecules onto HTNF. The experimental conditions were: MB

128   concentration 10 mg/L, pH = 9 (after adding the powder no pH adjustment was done) and T =

129   25 °C.

130

131   2.3.2. Effect of MB Concentration

132

4

133   After optimising the HTNF loading, three MB concentrations (5, 10 and 20 mg/L) were

134   selected to study the kinetics of adsorption. The experiment was performed under the

135   following conditions: HTNF = 0.5 g/L, pH = 9 and T = 25 °C.

136

137   2.3.3. Effect of pH

138

139   The pH of the solution is known to affect the surface charge of the nanofibres, and

140   consequently the adsorption of dye molecules. The experiment was conducted at the pH

141   values of 3, 5, 7 and 9 while all other factors were kept constant at HTNF = 0.5 g/L, MB = 20

142   mg/L and T = 25 °C.

143

144   2.3.4.   Effect of Solution Temperature

145

146   The temperature of the solution was changed to study its effect on the adsorption process. In

147   these experiments the selected temperatures were 25, 35, and 45 °C. The experimental

148   conditions were: HTNF = 0.5 g/L, MB = 20 mg/L, and pH = 9.

149

150   2.3.5.   Adsorption Equilibrium and Isotherms

151

152   The amount of dye adsorbed at equilibrium was calculated from the following equation:

153

154   $$q_e = (C_0 - C_e)\frac{V}{m}$$ (Eq. 2)

155

156   where, C_0 and C_e (mg/L) are the initial and equilibrium concentration of MB in solution, V

157   (L) is the solution volume and m (g) is the mass of the HTNF.

158

159   Sorption equilibrium data were fitted to the Langmuir, Freundlich, and Toth models using

160   both linearised and nonlinear parameter estimations. The Langmuir isotherms showed good

161   correlations, while the Toth model showed significantly low fit ($R^2 = 0.70$) for HTNF loading

162   data. The Freundlich model poorly predicted the effect of MB concentration ($R^2 = 0.48$), and

163   was inappropriate ($R^2 = 0.09$) for HTNF loading data. Therefore, in this study the Langmuir

164   isotherm model was employed for data analysis, using a simple yet sufficiently accurate

165   linearised form (Langmuir, 1918):

166

167

168
$$\frac{C_e}{q_e} = \frac{1}{kq_m} + \frac{1}{q_m}C_e$$
(Eq. 3)

169

170 where, C_e is the equilibrium concentration, q_e (mg/g) is the amount of adsorbate adsorbed on

171 unit mass of adsorbent, q_m (mg/g) and k (L/mg) are the Langmuir adsorption constants related

172 to adsorption capacity and rate of adsorption, respectively. The q_m and k values were

173 calculated from the slope and intercept of the straight line obtained after plotting C_e/q_e against

174 C_e, respectively.

175

176 **2.4.   Photocatalytic Degradation under Simulated Solar Light**

177

178 The photocatalytic activity of HTNF (0.5 g/L) was assessed using 200 mL volume of MB

179 solution (20 mg/L). The HTNF loading and MB concentration were selected based on the

180 results obtained in the adsorption experiments. The effect of solution pH (3, 5, 7 and 9) and

181 solar light intensity (5000, 15000 and 28000 lx; measured by a digital power meter AR 823)

182 on the removal of MB were studied. MB molecules were adsorbed on HTNF in dark after

183 mixing at 450 rpm for 30 min. The solution was then placed in the Solar Simulator (SolSim,

184 Luzchem Research, Canada) and photocatalysis was carried out for 180 min at a stable

185 temperature of 26 ℃. The Luzchem Research SolSim Xenon photoreactor featured an

186 enclosed exposure chamber, an exhaust system and thermostatic control to maintain the

187 chamber temperature close to ambient temperature. The principal light source was a Xenon

188 lamp (300 W) and a complex filter system ensured emission to closely match the AM1.5

189 spectrum. Air sparging was adjusted at 0.6 L/min to provide adequate dissolved oxygen to the

190 reaction. MB degradation was monitored by collecting samples (filtered by 0.45 µm PTFE

191 syringe filters) at fixed time intervals and analysed for colour removal at $\lambda = 664$ nm using a

192 Shimadzu UV-Vis 1700 spectrophotometer. Samples were also analysed for dissolved

193 organic carbon (DOC) removal using a Multi N/C 3100, Analytik Jena instrument. The

194 kinetics of the photocatalytic discolouration (MB removal) and mineralisation (DOC

195 removal) reactions were analysed by nonlinear data fitting (OriginPro v8 software,

196 OriginLab) to the equation:

197

198 $C_t = C_0 \cdot e^{-k_a \cdot t}$ (Eq. 4)

199

200 where, C_t (mg/L) is the concentration of MB or DOC at time t, C_0 (mg/L) is the initial

201 concentration of MB or DOC, t is time, and k_a is the apparent pseudo first order constant.

202

203 **2.5. Photocatalytic Stability**

204

205 The photocatalytic stability of HTNF (0.5 g/L) was examined over three successive cycles

206 using 200 mL volume of MB solution (20 mg/L). The pH of the solution was 9 and air

207 sparging was adjusted to a rate of 0.6 L/min at a light intensity of 28000 lx. At the end of

208 each cycle (for 8 h to ensure complete regeneration), HTNF were recovered and washed with

209 MQ water before being used in the next degradation cycle. Samples were also analysed for

210 changes in absorbance at 254 nm and 664 nm wavelengths, and for DOC removal.

211

212 **2.6. Photocatalyst Separation by Settling**

213

214 The separation of HTNF in MQ water by gravity settling was studied in 200 mL beaker by

215 collecting samples from 5 cm below the water surface (HTNF = 0.5 g/L, pH = 9). Sample

216 turbidity was logged over time and measured using the Hach HI 93414 turbidity and chlorine

217 meter.

218

3. Results and Discussion

3.1.1. Characteristics of H-titanate Nanofibres

221

Figure 1 shows the zeta potential of the as-prepared and calcined HTNF. The calcination shifted the PZC towards higher pH due to the evaporation of peroxo groups (O_2^-, adsorbed H_2O_2 etc). While the properties of the as-prepared titanate will not be discussed in this study, its zeta potential characteristics are useful to elucidate the noticed shift of pH after calcination.

227

SEM images of HTNF revealed fibrous nanostructures of randomly dispersed nanofibres with an average diameter of 40-70 nm and few hundred nanometers in length (Figure 2). The length and width of nanofibres were averaged from twenty measurements recorded after image capture using a measuring tool provided by the Zeiss Supra 55VP SEM/EDS instrument software. It has been discussed previously (El Saliby et al., 2011a) that the Na-titanate nanofibres were arranged in microspheres of few micrometres in diameter. In contrast, the acid wash at low pH (ion exchange) affected the aggregation of nanofibres but the nanofibres conserved their typical morphology; the latter has also been observed by several researchers (Wei et al., 2004; Zhu et al., 2004; Bela et al., 2010).

237

Figure 1

239

Figure 2

241

The characteristic peaks in the EDS spectrum of HTNF (Figure 3) reveal the presence of only titanium and oxygen. This result indicates the effective exchange of Na^+ for H^+ prior to calcination.. The XRD analysis showed that the nanofibres were mainly anatase (data not shown). The calculated surface area of nanofibres was 31.54 m^2/g, the average pore volume 0.10 cm^3/g and average pore size 50 Å.

247

Figure 3

249

3.1.2. Effect of Operating Conditions on MB Adsorption

3.1.2.1. Effect of HTNF Loading

8

252

253 The effect of HTNF loading on the removal of MB from the solution was studied using

254 photocatalyst loadings of 0.1, 0.2, 0.5, 1 and 2 g/L. The results of experiments carried out at

255 25 ℃ and 10 mg/L of MB are shown in Figure 4. The adsorption of MB increased with

256 photocatalyst loading until equilibrium was reached after 30 min. An increase in HTNF

257 dosage from 0.1 to 0.5 g/L increased the adsorption of MB from 11% to a remarkably high

258 90%. The increase in the adsorption efficiency can be explained by the increase in the surface

259 area available for adsorption. However, no significant increase in adsorption was recorded

260 after increasing the loading to 1 and 2 g/L (92% and 93%, respectively). This could be

261 attributed to the attainment of adsorption equilibrium between MB and HTNF, or reaching

262 the adsorption saturation point. The photocatalyst loading of 0.5 g/L was considered optimum

263 and was adopted for the next optimisation process.

264

265 **Figure 4**

266

267 3.1.2.2. Effect of Initial MB Concentration

268

269 Figure 5 shows the adsorption of MB onto HTNF using initial MB concentrations of 5, 10

270 and 20 mg/L. It is evident that the initial MB concentration played a significant role in the

271 adsorption process, where 97%, 89% and 42% of MB were removed at MB concentrations

272 equal to 5, 10 and 20 mg/L, respectively. The HTNF removed almost all the dye at relatively

273 low initial concentration. In industrial applications, high MB removal at low concentrations is

274 considered to be of a great importance. The amount of MB adsorbed increased with time until

275 the equilibrium was attained at 30 min for high MB concentrations (10 and 20 mg/L), while

276 almost all MB molecules were adsorbed within 5 min at 5 mg/L of MB. The initial uptake

277 (first few minutes) for MB was high because a large number of adsorption sites were

278 available for adsorption. Later on, the adsorption decreased as the repulsive forces between

279 the adsorbed MB molecules (on HTNF) and the MB molecules in the solution increased

280 (Fetterolf et al., 2003; Xiong et al., 2010). In order to study the effect of other parameters in

281 the adsorption process such as pH and temperature, 20 mg/L MB concentration was selected

282 and will be discussed in the following sections.

283

284 **Figure 5**

285

9

286   3.1.2.3. Effect of Solution pH

287

288   The adsorption of MB was studied in a suspension of 0.5 g/L of HTNF and 20 mg/L of MB

289   using different pH values (3, 5, 7 and 9). The results of adsorption are shown in Figure 6. MB

290   is a cationic dye which is favourably adsorbed on negatively charged surfaces (Feetrolf et al.,

291   2003). The zeta potential measurements of HTNF revealed that the surface charge of the

292   nanofibres was negative over a wide pH range, and that the PZC was around pH 3.2. At pH 3,

293   the repulsive forces between the HTNF and MB molecules dominated the adsorption process,

294   leading to a low overall adsorption (7% after 30 min). In contrast, when the pH was increased

295   to 5, 7, and 9, MB adsorption increased to 28%, 32% and 42%, respectively. This was mainly

296   due to electrostatic attraction between the HTNF surface and MB molecules. This finding

297   was in agreement with previous studies on the adsorption of MB onto titania (Fetterolfet al.,

298   2003), titanate nanotubes (Xiong et al., 2010) and different organic and inorganic adsorbent

299   (Ai et al., 2011).

300

301   **Figure 6**

302

303   3.1.2.4. Effect of Solution Temperature

304

305   The effect of different solution temperatures on the adsorption is shown in Figure 7. The

306   adsorption of MB increased with temperature increase, indicating an endothermic adsorption

307   process (Bulut and Aydin, 2006; Hong et al., 2009). The total adsorption at equilibrium (30

308   min) was found to increase from 42% to 52% for an increase in the solution temperatures

309   from 25 to 45 ℃.

310

311   **Figure 7**

312

313   3.1.2.5. Adsorption Equilibrium and Isotherms

314

315   Figures 8A and 8B show the amount of MB adsorbed at equilibrium (30 min) using different

316   HTNF loadings and MB concentrations, respectively. The adsorption of dye increased with

317   HTNF loading to a maximum of 17.8 mg/g at 0.5 g/L and then decreased to 9.18 and 4.64

318   mg/g at 1 and 2 g/L, respectively. The increase in the adsorption capacity (q_e) reached a

319   maximum at 0.5 g/L of HTNF loading while further increase in the mass of HTNF

10

320 (denominator in Eq.2) with $(C_0-C_e)*V$ (Eq. 1) remaining constant caused the decrease in q_e.

321 The effect of initial MB concentration revealed that the increase of MB concentration at a

322 constant HTNF loading increased the adsorption mainly because of high driving force for

323 mass transfer (Bulut and Aydin, 2006). The data plotted in Figure 8B showed some decrease

324 in q_e after increasing the concentration of MB from 10 to 20 mg/L (data collected after 30

325 min of contact). However, the experiments were continued for 3 h and no significant

326 difference in q_e at MB concentrations of 10 mg/L and 20 mg/L was found (q_e for both

327 concentrations varied from 16.5 to 17.8 mg/g).

328

329 **Figure 8**

330

331 During adsorption, the adsorption capacity is highly influenced by the pH variations of the

332 solution (Wang et al., 2005). The plot of pH variation against the adsorption capacity is

333 shown in Figure 9A. The adsorption capacity increased from 2.55 mg/g at pH 3 to 16.57

334 mg/g at pH 9 after 30 min of contact. As discussed earlier, the surface charge of HTNF

335 changed from positive to negative at pH 3 and 9, respectively. This played an important role

336 in adsorbing more cationic MB molecule at high pH.

337

338 Increasing the temperature of the solution enhanced the adsorption of MB molecules onto

339 HTNF (Figure 9B). The adsorption capacity increased from 16.57 mg/g at 25 °C to 19 mg/g

340 at 45 °C. It has been discussed earlier in this study that the process of adsorption is

341 endothermic. The heat of adsorption can describe the physical or chemical adsorption of gas

342 molecules into solid surfaces (Sircar, 2005). Nevertheless, the use of endothermic and

343 exothermic adsorption terminologies to explain adsorption in water has been widely accepted.

344

345 To further describe the equilibrium of adsorption, the most commonly used adsorption model

346 (Langmuir) has been used to fit the data obtained under different operating conditions. The

347 data was fitted using Eq. 3 and the results are shown in Table 1. Our data fitted well the

348 Langmuir model. The goodness of fit was shown with R^2 equal to 0.99, 0.91, 0.89 and 0.99

349 for experiments on HTNF loading, MB concentration, pH and temperature, respectively.

350 These findings indicated that the monolayer adsorption of MB on HTNF was the dominant

351 mechanism of adsorption. The Langmuir model has fitted well the adsorption data of MB

352 onto titanate nanotubes (Xiong et al., 2010). It has been reported that uniform nanotubular

11

353 structure and homogenous distribution of active sites on the walls favoured this adsorption

354 mechanism.

355

356 **Figure 9**

357

358 **Table 1**

359

360 The Langmuir isotherm was further evaluated by the dimensionless constant separation factor

361 R_L (Hall et al., 1966; Weber and Chakravorti, 1974):

362

363
$$R_L = \frac{1}{1+kC_0}$$
(Eq. 5)

364

365 With k Langmuir constant (L/mg) and C_0 initial MB concentration (mg/L). The value of R_L

366 indicates the shape of the adsorption isotherm and values between 0 and 1 indicate favourable

367 adsorption (McKay et al., 1982). The calculated R_L from our data showed values between 0

368 and 1 suggesting that the adsorption between MB and HTNF was favourable (Table 2).

369 Moreover, low R_L values (<0.04) indicated that the interaction between MB and HTNF was

370 relatively strong (Xiong et al., 2010).

371

372 **3.1.3. Photocatalytic Decolourisation and DOC Removal of MB**

373 3.1.3.1. Effect of Solution pH

374

375 The variation of solution pH directly influenced the adsorption of MB molecules onto HTNF

376 through electrostatic interactions. The adsorption was favoured at high pH between different

377 surface charges and decreased with pH decrease. Figure 10 shows the discolouration and the

378 DOC removal of MB solution after 30 min adsorption and 180 min of light irradiation. The

379 discolouration of the solution was almost complete after 90 min for pH values of 5, 7 and 9.

380 In contrast, only 89% of MB was removed after 180 min of light irradiation at pH 3. The

381 decrease in DOC was slower being 48%, 75%, 78% and 78% for pHs of 3, 5, 7 and 9. The

382 results of regression analysis between MB discolouration and DOC removal are presented in

383 Table 3.

384

385 The effect of solution pH on the discolouration of MB solution was reported in the literature

386 (Shimizu et al., 2007; Tayade et al., 2009). Shimizu et al. (2007) found that the change of pH

387 between 3 and 10 did not influence the solution colour in the absence of the photocatalyst.

388 However, significant decrease in colour was reported at pH above 10. In this study, the pH

389 range was between 3 and 9, thus it can be assumed that the initial concentration of MB was

390 constant. Moreover, photodegradation data collected in different experiments were

391 normalised to the initial MB absorbance measured at pH values of 3, 5, 7 and 9. Lachheb et

392 al. (2002) studied the adsorption of several dyes, including MB, onto TiO_2 under different pH

393 values ranging from 3 to 9. In agreement with the present findings, they also reported low

394 MB adsorption at low pH but little influence of pH variations upon the kinetics of colour

395 disappearance under UV light. In another study on MB photodegradation, Wu and Chern

396 (2006) showed that increasing the pH above the PZC of TiO_2 (PZC $\approx$ 4.5 according to

397 authors' measurements) has dramatically impacted the dispersion of particles in solution,

398 leading to coagulation and sedimentation. Consequently, the decomposition of MB was

399 decreased because of the decrease in TiO_2 surface area. In this study, no coagulation of

400 HTNF was observed but the decrease of adsorption (at pH 3) retarded the discolouration.

401 This observation indicates that the decomposition of MB molecules was due to the attack by

402 the $OH^{\bullet}$ radicals near the HTNF surface under these conditions. In contrast, surface

403 degradation was the dominating degradation mechanism at high solution pH.

404

405 **Figure 10**

406

407 **Table 3**

408

409 3.1.3.2. Effect of Light Intensity

410

411 The effect of light intensity on the photodegradation of MB was studied and the results are

412 shown in Figure 11. The light intensity of the system can affect the electron/hole formation,

413 their separation and recombination rate. However, this can also be affected by the emitted

414 wavelength of the lamp and the type of photocatalyst. In the reactor used in the present

415 experiments, the decrease of light intensity from 28000 lx to 15000 lx did not significantly

416 decrease the degradation rate of MB after 180 min of light irradiation. However, a further

417 reduction in light intensity to 5000 lx resulted in 25% decrease in discolouration efficiency of

13

418   the system (adsorption + photodegradation). DOC removal of the system was high (78%) for

419   the maximum intensity (28000 lx), decreasing to 73% at 15000 lx and to 64% at 5000 lx.

420

421   The pseudo-first order apparent constants are shown in Table 4. These were calculated by

422   using the decrease in MB concentration (k^1_a) and the decrease of solution DOC (k^2_a) over

423   time. k^1_a values increased from 0.011 min^{-1} at pH 3 to 0.034 min^{-1} at pH 9. Similarly, k^1_a

424   increased from 0.0037 min^{-1} to 0.034 min^{-1} with the increase in light intensity. The

425   photodiscolouration of MB over HTNF followed the pseudo-first order reaction kinetics,

426   noting that similar finding was reported by Houas et al. (2001) for photodegrading MB over

427   Degussa P25.

428

429   **Figure 11**

430

431   k^2_a was calculated from the DOC concentration decrease over time (Table 4). DOC removal

432   kinetics were slower than those observed for MB discolouration and this could be attributed

433   to the formation of photodegradation intermediates (Herrmann, 1999; Houas et al., 2001;

434   Lachheb et al., 2002). The apparent rate constant increased with pH and light intensity

435   increase. The adsorption of MB onto HTNF favoured its photocatalytic removal from the

436   solution at basic pH (Houas et al., 2001).

437

438   **Table 4**

439

440   **3.1.4. Photocatalytic Stability of HTNF**

441

442   The photocatalytic stability of HTNF was also tested by adopting the experimental model of

443   Xiong et al. (2011). The experiments consisted of running photocatalytic degradation

444   reactions without the dark adsorption of MB onto HTNF. A 200 mL beaker containing 0.1 g

445   of HTNF suspended in 20 mg/L MB solution was placed in the solar simulator at 28000 lx

446   and at a temperature of 26 °C.

447

448   Figures 12 and 13 show the normalised photocatalytic degradation data obtained from the

449   absorbances at λ = 254 nm and 664 nm. The MB solution changed to colourless after 2 h of

450   photoreaction, then turned to humic-like water colour between 2 h to 6 h before becoming

14

451 colourless at the end (after almost 8 h). These findings suggest that the photocatalytic
452 degradation of MB in this system has occurred in three stages:

453 • Stage 1: Concurrent adsorption of MB and photocatalytic degradation to
454 positively charged intermediates (surface reaction) (Houas et al., 2001; Orendorz
455 et al., 2008).
456 • Stage 2: Desorption of intermediate compounds, (mainly negatively charged
457 phenolic or aromatic organics) from HTNF surface (Houas et al., 2001).
458 • Stage 3: Degradation of aromatic intermediates by OH$^\bullet$ attacks.

459

460 The experiments were repeated using the recycled photocatalyst over three degradation
461 cycles, with no significant changes in photocatalytic activity (Figure 14).

462

463 **Figure 12**

464

465 **Figure 13**

466

467 **Figure 14**

468

469 **3.1.5. Settling Characteristic of HTNF**

470

471 The high cost associated with the separation of titania at commercial scale has seriously
472 retarded the use of industrial photocatalysis. At the end of photocatalysis, the facile recovery
473 of the photocatalyst is very important for its reuse. A low cost catalyst separation process can
474 be achieved by settling of particles. Accordingly, the settling characteristics of HTNF were
475 also evaluated by comparing the sedimentation of HTNF to Degussa P25 in aqueous
476 suspensions (Figure 15). The catalyst concentration was 0.5 g/L at a pH of 9. Rapid HTNF
477 sedimentation was recorded by measuring the turbidity of decanted solution at fixed time
478 intervals. About 80% turbidity removal was achieved after 30 min of settling that increased
479 up to 90% after 2 h settling time. In contrast, the turbidity of P25 suspension did not change
480 significantly. In a similar study, Xiong et al. (2011) reported 72% decrease in turbidity within
481 180 min settling time for titanate nanotubes (0.5 g/L titanate loading in a 300 mL square
482 photoreactor). The rapid sedimentation of HTNF is another advantage for their industrial
483 application in wastewater photocatalysis.

484

485   **Figure 15**

486

487

488   **4. Conclusions**

489

490   H-titanate nanofibres were synthesised by an aqueous peroxide route at high pH. The HTNF

491   were characterised for changes in morphology by observing SEM images which revealed

492   randomly dispersed nanofibres with an average diameter of 40-70 nm and few hundred

493   nanometers in length. The nanofibres were negatively charged over a wide pH range and their

494   PZC was found at pH 3.2. H^+ successfully replaced Na^+ in the nanofibres by ion exchange as

495   confirmed by EDS measurements. The HTNF were mainly anatase with a surface area of

496   31.54 m^2/g, average pore volume of 0.10 cm^3/g and average pore size of 50 Å.

497

498   The adsorption of MB onto HTNF was examined by investigating the effect of HTNF

499   loading, MB concentration, solution pH, and temperature on the adsorption capacity. The

500   results showed that the adsorption of MB was promoted by high catalyst loadings, high pH

501   (greater than the PZC) and temperature. The adsorption capacity increased from 2.55 mg/g at

502   pH 3 to 16.57 mg/g at pH 9 after 30 min of contact, and from 16.57 mg/g at 25 °C to 19 mg/g

503   at 45 °C. The adsorption data fitted well the Langmuir model for all operational conditions.

504   The optimum operational conditions for the adsorption of MB onto HTNF were found at 0.5

505   g/L of photocatalyst, 10 mg/L MB, pH 9 and temperature of 45 °C.

506

507   The photocatalytic degradation of MB was studied under simulated solar light to study the

508   effect of pH and light intensity. No significant differences were found for the discolouration

509   of MB at pHs greater than the PZC. However, at pH 3, the decrease in MB adsorption

510   significantly reduced its consecutive photocatalytic degradation. The increase in light

511   intensity from 5000 lx to 28000 lx was found to increase 10 folds the discolouration of MB,

512   according to the apparent degradation constant (k^1_a) obtained from the L-H model. In

513   contrast, the DOC removal at the highest light intensity was only twice as good as the DOC

514   removal found at the lowest light intensity (k^2_a).

515

16

516 The photocatalytic activity of the nanofibres was found stable after 3 degradation cycles

517 using the adsorption/photocatalysis model. Moreover, the fibres were easily separated from

518 the solution by settling at room temperature.

519

520

521

522 **Acknowledgment**

527

528 **References**

529

530 Ai, L., Li,M.,Li, L., 2011. Adsorption of methylene blue from aqueous solution with
531   activated carbon/cobalt ferrite/alginate composite beads: kinetics, isotherms, and
532   thermodynamics. Journal of Chemical and Engineering Data 56(8), 3475-3483.

533 Baiju, K.V., Shukla, S., Biju, S., Reddy, M.L.P., Warrier, K.G.K., 2009. Hydrothermal
534   processing of dye-adsorbing one-dimensional hydrogen titanate. Materials Letters
535   63(11), 923-926.

536 Bela, S., Wong, A.S.W. and Ho., G.W., 2010. Hydrolysis and ion exchange of titania
537   nanoparticles towards large-scale titania and titanate nanobelts for gas sensing
538   applications. Journal of Physics D: Applied Physics 43(3), 035401.

539 Bulut, Y., Aydin, H., 2006. A kinetics and thermodynamics study of methylene blue
540   adsorption on wheat shells. Desalination 194, 259-267.

541 El Saliby, I., Erdei, L., Shon, H.K., Kim, J.B., Kim, J.-H., 2011a. Preparation and
542   characterisation of mesoporous photoactive Na-titanate microspheres. Catalysis
543   Today 164(1), 370-376.

544 El Saliby, I., Shon, H.K., Kandasamy, J., Kim, J.-H., 2011b. Synthesis, characterisation and
545   separation of photoreactive Hydrogen-titanate nanofibrous channel. Separation
546   Purification Technology 77(2), 202-207.

547   Fetterolf, M.L., Patel, H.V., Jennings, J.M., 2003. Adsorption of methylene blue and acid
548   blue 40 on titania from aqueous solution. Journal of Chemical and Engineering Data
549   48(4), 831-835.

550   Hall, K.R., Eagleton, L.C., Acrivos, A., Vermeulen, T., 1966. Pore- and solid-diffusion
551   kinetics in fixed-bed adsorption under constant-pattern conditions. Industrial and
552   Engineering Chemistry Fundamentals 5(2), 212-223.

553   Herrmann, J.-M., 1999. Heterogeneous photocatalysis: fundamentals and applications to the
554   removal of various types of aqueous pollutants. Catalysis Today 53(1), 115-129.

555   Hong, S., Wen, C., He, J., Gan, F. andHo, Y.-S., 2009. Adsorption thermodynamics of
556   methylene blue onto bentonite. Journal of Hazardous Materials 167, 630-633.

557   Houas, A., Lachheb, H., Ksibi, M., Elaloui, E., Guillard, C., Herrmann, J.-M., 2001.
558   Photocatalytic degradation pathway of methylene blue in water. Applied Catalysis B:
559   Environmental 31(2), 145-157.

560   Lachheb, H., Puzenat, E., Houas, A., Ksibi, M., Elaloui, E., Guillard, C., Herrmann, J.-M.,
561   2002. Photocatalytic degradation of various types of dyes (Alizarin S, Crocein Orange
562   G, Methyl Red, Congo Red, Methylene Blue) in water by UV-irradiated titania.
563   Applied Catalysis B: Environmental 39(1), 75-90.

564   Langmuir, I., 1918. The adsorption of gases on plane surfaces of glass, mica and platinum.
565   Journal of the American Chemical Society 40(9), 1361-1403.

566   Lee, C.-K., Lin, K.-S., Wu, C.-F., Lyu, M.-D., Lo, C.-C., 2008a. Effects of synthesis
567   temperature on the microstructures and basic dyes adsorption of titanate nanotubes.
568   Journal of Hazardous Materials150(3), 494-503.

569   Lee, C.-K., Liu, S.-S., Juang, L.-C., Wang, C.-C., Lyu, M.-D., Hung, S.-H., 2007.
570   Application of titanate nanotubes for dyes adsorptive removal from aqueous solution.
571   Journal of Hazardous Materials148(3), 756-760.

572   Lee, C.-K., Wang, C.-C., Juang, L.-C., Lyu, M.-D., Hung, S.-H., Liu, S.-S., 2008b. Effects of
573   sodium content on the microstructures and basic dye cation exchange of titanate
574   nanotubes. Colloids and Surfaces A: Physicochemical and Engineering Aspects 317,
575   164-173.

576   Mao, Y., Kanungo, M., Hemraj-Benny, T., Wong, S.S., 2006. Synthesis and growth
577   mechanism of titanate and titania one-dimensional nanostructures self-assembled into
578   hollow micrometer-scale spherical aggregates. The Journal of Physical Chemistry B
579   110(2), 702-710.

18

580   McKay, G., Blair, H.S.,Gardner, J.R., 1982. Adsorption of dyes on chitin. I. Equilibrium
581   studies. Journal of Applied Polymer Science 27(8), 3043-3057.

582   Nyman, M., Hobbs, D.T., 2006. A Family of Peroxo-titanate Materials Tailored for Optimal
583   Strontium and Actinide Sorption. Chemistry of Materials 18(26), 6425-6435.

584   Orendorz, A., Ziegler, C.,Gnaser, H., 2008. Photocatalytic decomposition of methylene blue
585   and 4-chlorophenol on nanocrystalline TiO_2 films under UV illumination: A ToF-
586   SIMS study. Applied Surface Science 255(4), 1011-1014.

587   Sircar, S. (2005) Heat of adsorption on heterogeneous adsorbents. Applied Surface Science
588   252(3), 647-653.

589   Shimizu, N., Ogino, C., Dadjour, M.F., Murata, T., 2007. Sonocatalytic degradation of
590   methylene blue with TiO_2 pellets in water. Ultrasonics Sonochemistry 14(2), 184-190.

591   Tayade, R.J., Natarajan, T.S., Bajaj, H.C., 2009. Photocatalytic degradation of methylene
592   blue dye using ultraviolet light emitting diodes. Industrial and Engineering Chemistry
593   Research 48(23), 10262-10267.

594   Wang, S., Boyjoo, Y.,Choueib, A., 2005. A comparative study of dye removal using fly ash
595   treated by different methods. Chemosphere 60(10), 1401-1407.

596   Weber, T.W.,Chakravorti, R.K., 1974. Pore and solid diffusion models for fixed-bed
597   adsorbers. AIChE Journal 20(2), 228-238.

598   Wei, M., Konishi, Y., Zhou, H., Sugihara, H., Arakawa, H., 2004. A simple method to
599   synthesize nanowires titanium dioxide from layered titanate particles. Chemical
600   Physics Letters 400, 231-234.

601   Wu, C.-H.,Chern, J.-M., 2006. Kinetics of photocatalytic decomposition of methylene blue.
602   Industrial and Engineering Chemistry Research 45(19), 6450-6457.

603   Xiong, L., Sun, W., Yang, Y., Chen, C.,Ni, J., 2011. Heterogeneous photocatalysis of
604   methylene blue over titanate nanotubes: Effect of adsorption. Journal of Colloid and
605   Interface Science 356(1), 211-216.

606   Xiong, L., Yang, Y., Mai, J., Sun, W., Zhang, C., Wei, D., Chen, Q., Ni, J., 2010. Adsorption
607   behavior of methylene blue onto titanate nanotubes. Chemical Engineering Journal
608   156(2), 313-320.

609   Zhu, H., Gao, X., Lan, Y., Song, D., Xi, Y.,Zhao, J., 2004. Hydrogen titanate nanofibers
610   covered with anatase nanocrystals: A delicate structure achieved by the wet chemistry
611   reaction of the titanate nanofibers. Journal of the American Chemical Society
612   126(27), 8380-8381.

19

Adsorption and photocatalytic degradation of Methylene Blue (MB) over Hydrogen-Titanate nanofibres produced by a peroxide method

Research highlights:

- Fabrication and characterisation of highly-adsorbent photoreactive nanofibres.
- Bench scale adsorption and photocatalysis experiments for process optimisation.
- Decomposition of MB under simulated solar light and regeneration of nanofibres.
- Effective separation of nanofibres from the aqueous clean water by settling.

List of Tables

Table 1

Parameters	Operational conditions			
	HTNF Loading	**MB concentration**	**pH**	**Temperature**
q_m(mg/g)	12	16.7	1.1	8.84
k (L/mg)	5.5	30	0.08	0.17
R^2	**0.91**	**0.99**	**0.89**	**0.99**

Table 2

Operational conditions	HTNF loading (g/L)	MB concentration (mg/L)			pH	Temp (°C)
		5	**10**	**20**		
R_L	0.018	0.00002	0.028	0.001	0.37	0.22

Table 3

Parameter	Solution pH			
	3	**7**	**5**	**9**
Linear Regression equation	$y^§ = 0.489x^* + 0.547$	$y^§ = 0.668x^* + 0.272$	$y^§ = 0.677x^* + 0.244$	$y^§ = 0.753x^* + 0.188$
R^2	0.906	0.966	0.942	0.958

§y represents normalised DOC

*x represents normalised absorbance

Table 4

Parameter	Operational conditions						
	pH				Light Intensity		
	3	5	7	9	28000	15000	5000
$k^1_a(\text{min}^{-1})^§$	0.011	0.025	0.037	0.034	same as pH 9	0.018	0.0037
R^2	0.994	0.828	0.915	0.893	same as pH 9	0.986	0.9440
$k^2_a(\text{min}^{-1})^*$	0.003	0.004	0.004	0.004	same as pH 9	0.003	0.002
R^2	0.979	0.820	0.888	0.735	same as pH 9	0.708	0.906

§Constants were calculated from the MB concentration degradation curves.

*Constants were calculated from the DOC degradation curves to include the degradation of intermediate compounds.

List of Figures

Figure 1

Figure 2

Figure 3

Figure 4
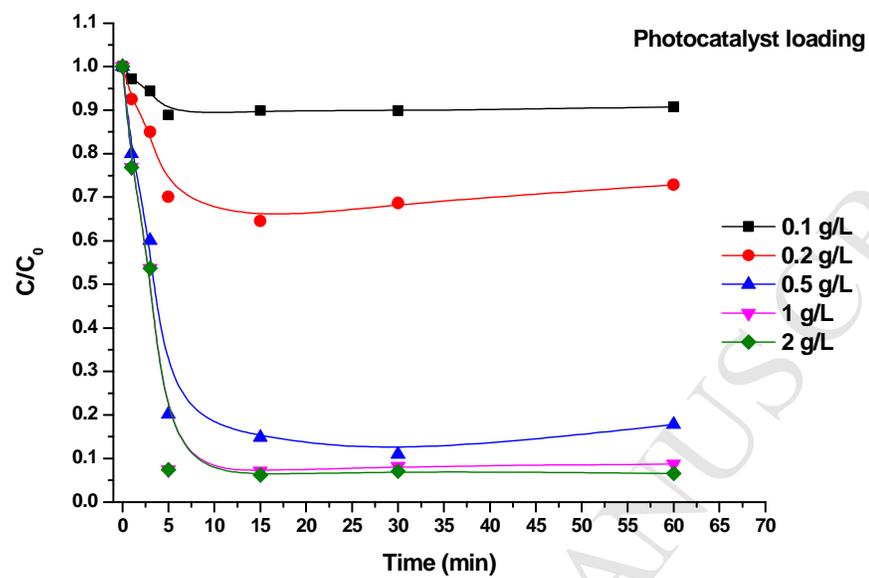
Figure 5
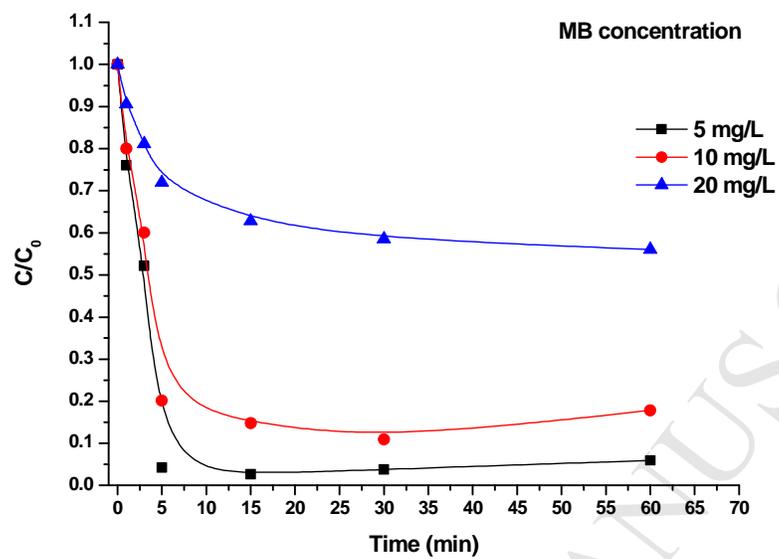
Figure 6
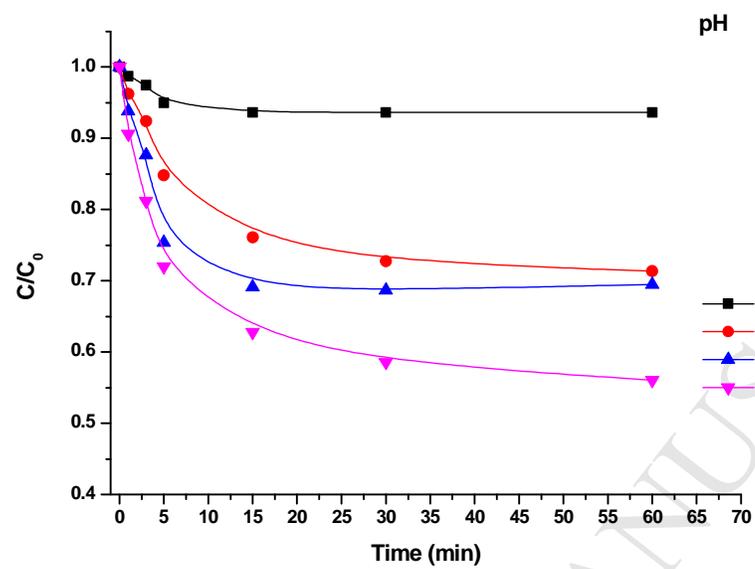
Figure 7
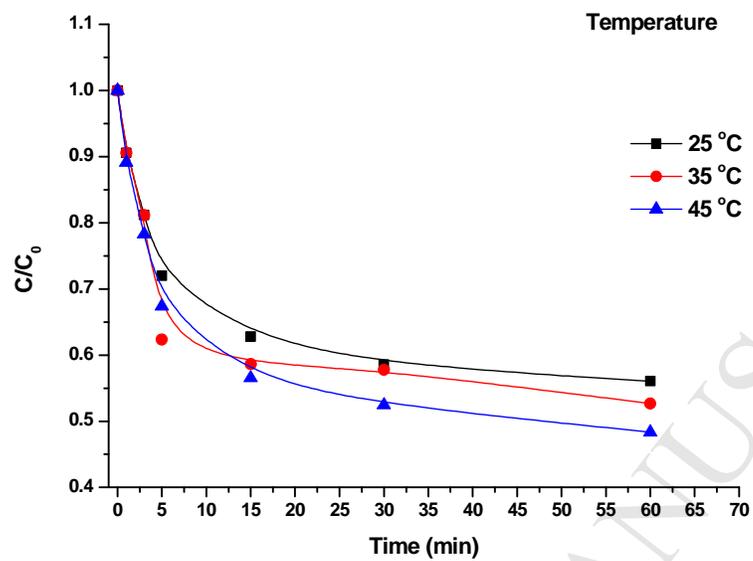
Figure 8
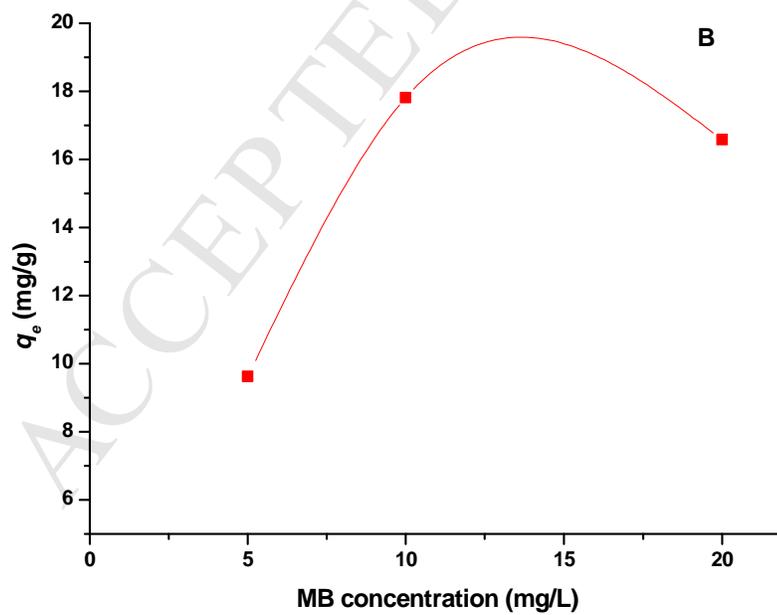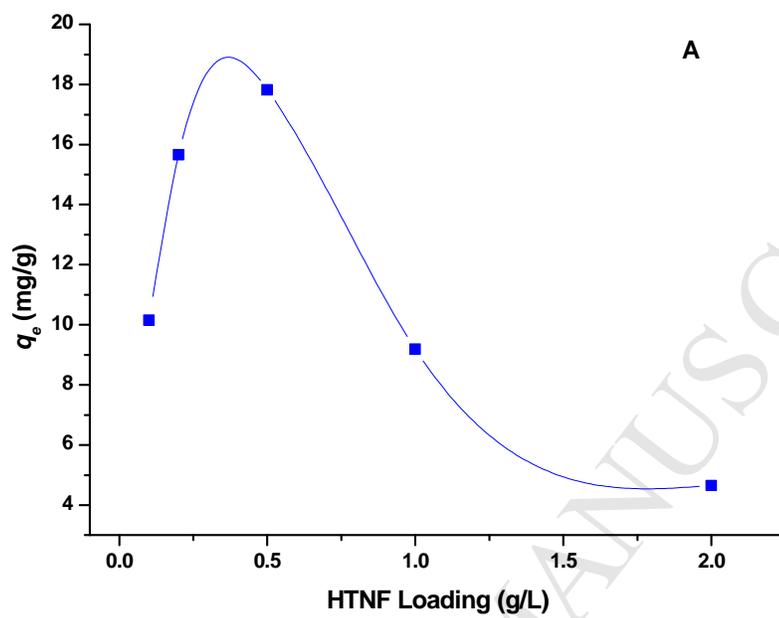
Figure 9
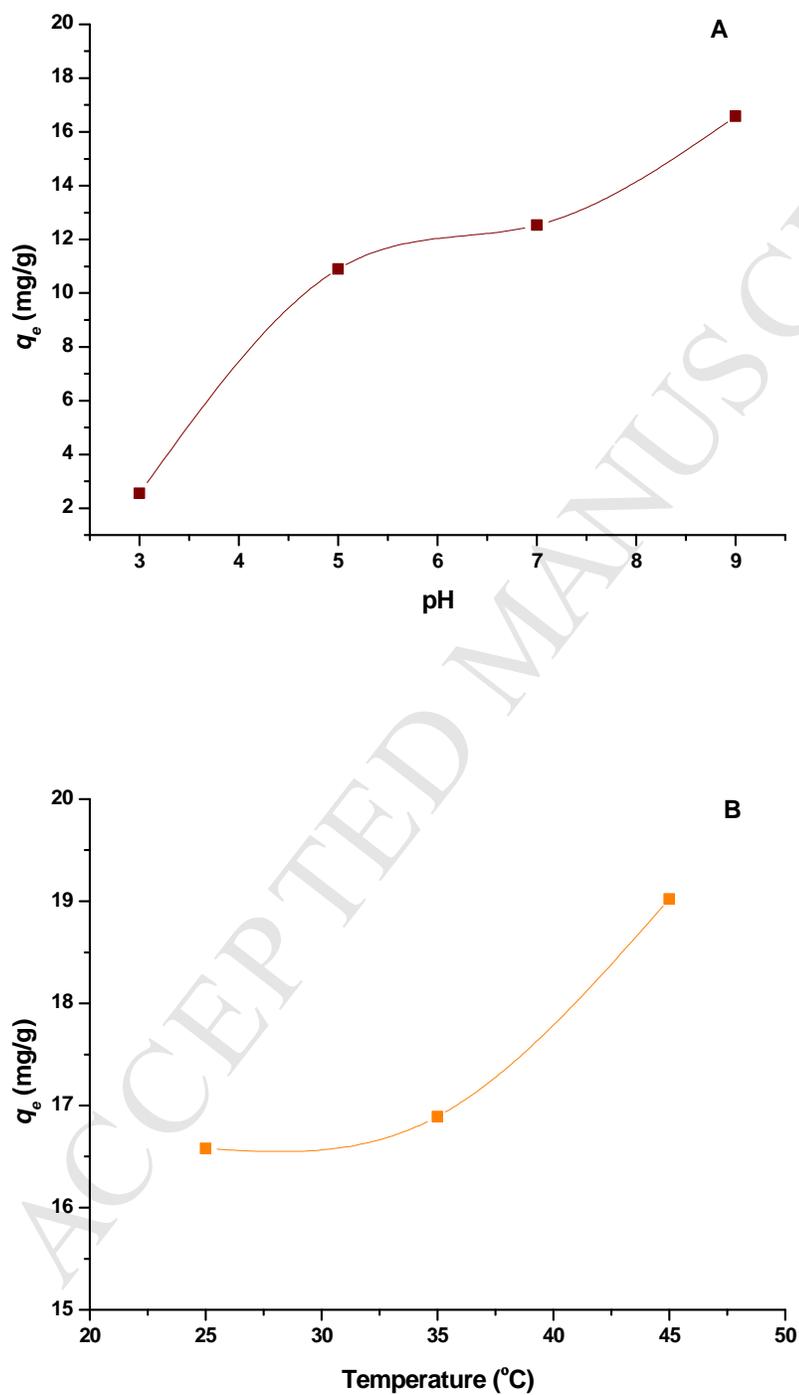
Figure 10
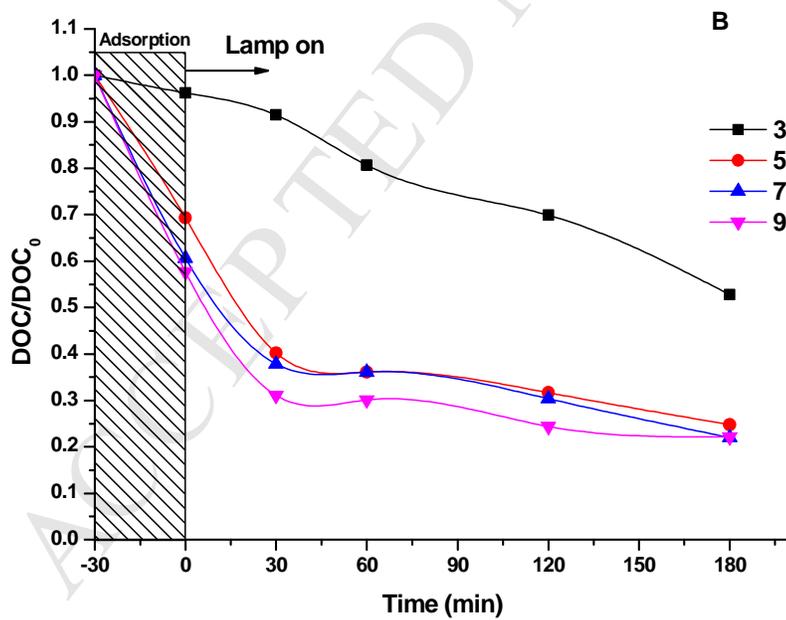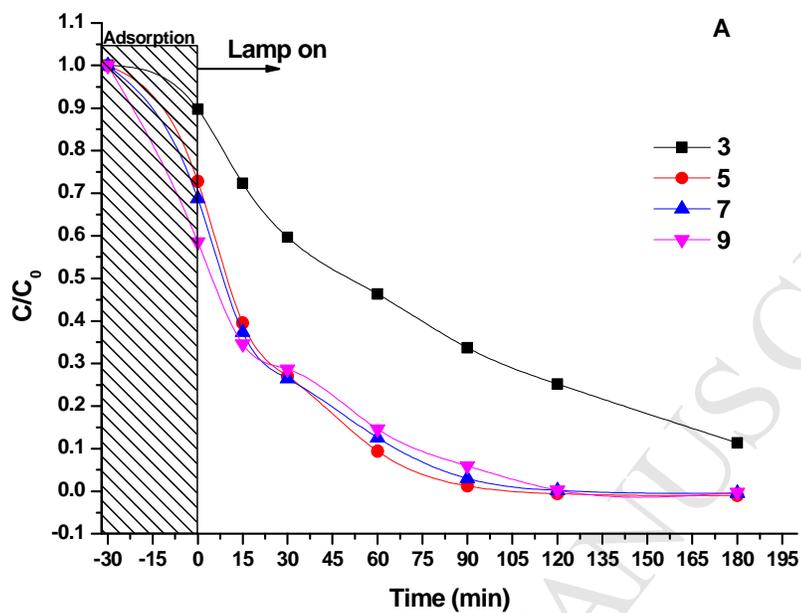
Figure 11
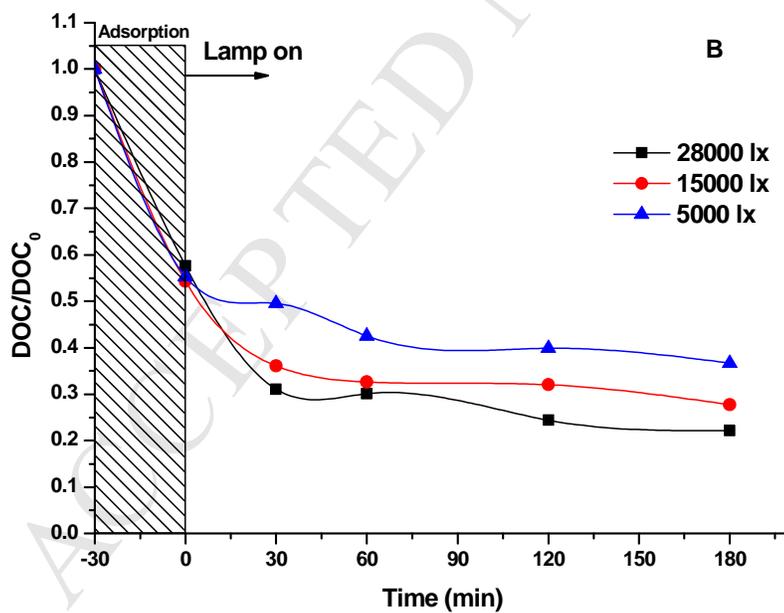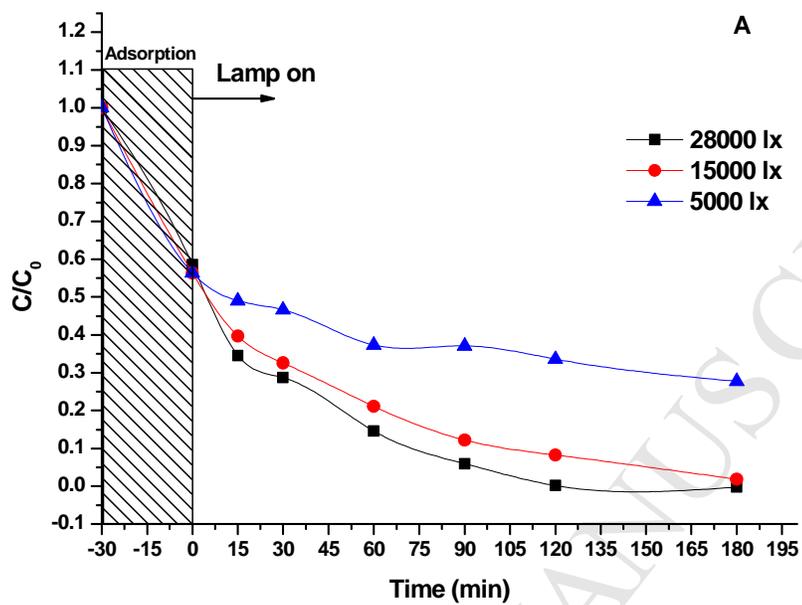
Figure 12
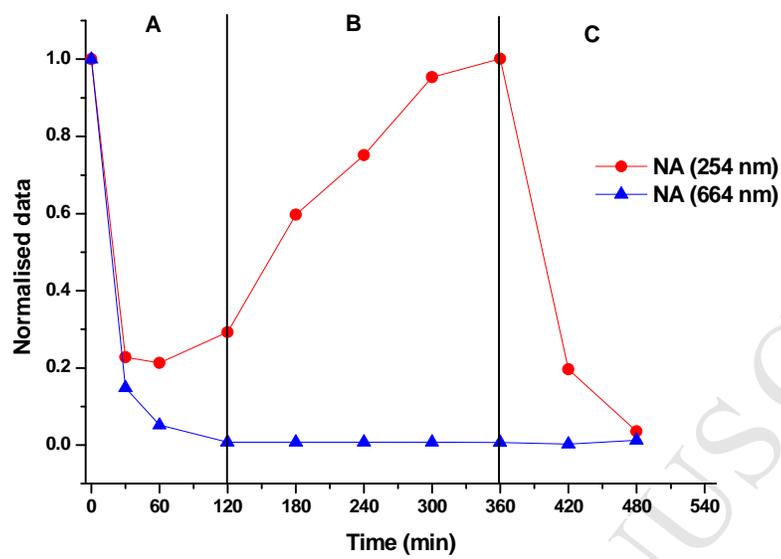
Figure 13

Figure 14

Figure 15